arXiv:astro-ph/0604493v1 24 Apr 2006

# A Survey of Merger Remnants III: Are Merger Remnants Supported by Rotation or Anisotropy? [1]

B. Rothberg

*Space Telescope Science Institute, 3700 San Martin Drive Baltimore, MD 21218*

rothberg@stsci.edu

R. D. Joseph

*Institute for Astronomy, 2680 Woodlawn Drive, Honolulu, HI 96822*

## ABSTRACT

A growing body of observational evidence suggests that the luminosity, photometric shape and amount of rotational or anisotropical support in elliptical galaxies may provide vital clues to how they formed. Elliptical galaxies appear to fall into two distinct categories based on these parameters: bright, boxy shaped, with little or no rotation, and less luminous, disky shaped with significant rotation. One viable formation scenario is the "Merger hypothesis," in which two disk galaxies merge to form a new elliptical galaxy. A comparison of the luminosity, photometric shape, and amount of rotation in advanced merger remnants may shed more light on the possible formation scenarios of elliptical galaxies. Yet, little observational data exists for such merger remnants. This paper is the third in a series investigating the photometric and kinematic properties of a sample of 51 *optically* selected advanced merger remnants. Presented here are $K$-band isophotal shapes and spatially resolved kinematics for a sub-sample of 37 merger remnants. The results show that $\sim 11\%$ of the sample are boxy, and anisotropically supported while $\sim 47\%$ are disky, and rotationally supported. The remainder of the sample show variations among expected correlations between shape and rotation. This may suggest that the isophotal shapes are still "in flux." There does appear to be a *lower* limit to the amount of anisotropy observed in the merger remnants. This *may* provide an observational diagnostic for discriminating among formation scenarios in elliptical galaxies.

*Subject headings:* galaxies: evolution—galaxies: formation—galaxies: interactions—galaxies: peculiar —galaxies: kinematics and dynamics—galaxies: structure

## 1. Introduction

Observations of elliptical galaxies reveal that they are far more complicated than first thought. Rather than being homogeneous ellipsoids flattened by rotation, photometry has shown that many elliptical galaxies exhibit isophotal deviations from perfect ellipses (e.g. Carter (1978); Lauer (1985)). Kinematic measurements indicate that some ellipticals show smaller than expected rotation (Illingworth 1977), while others appear to show significant rotation (Davies et al. 1983). Theoretical modeling has suggested that those which show smaller than expected rotation may be either triaxial in shape or flattened by anisotropy (Binney 1976, 1978). Isophotal shapes also appear to correlate with luminosity and rotation (Bender, Doebereiner, & Moellenhoff 1988; Bender et al. 1989), (hereafter BDM88 and B89). Follow-up studies have revealed that other properties such as X-ray and radio luminosities are correlated with boxy ellipticals, but not disky ellipticals (B89).

These observational results have formed a paradigm for classifying elliptical galaxies as either luminous, boxy-shaped, with little or no rotation (anisotropy), or faint, disky-shaped, with significant rotation. This now well-established dichotomy between "boxy" and "disky" ellipticals has fueled speculation that these properties are linked to different formation mechanisms. Kormendy & Bender (1996) and Kormendy & Djorgovski (1989) suggest a new morphological classification scheme in which ellipticals are categorized by their isophotal shapes. They argue that photometric shapes are a reliable measure of velocity anisotropy, which in turn is directly connected to how elliptical galaxies form. Furthermore, they suggest that disky isophotal shapes may be the result of gaseous dissipation which occurred during their formation. The origin of the dichotomy between boxy and disky ellipticals leads to the question of what role mergers may play in the formation of elliptical galaxies.

In the context of the Toomre Merger Hypothesis (Toomre & Toomre 1972; Toomre 1977) it is clear how disk-disk mergers can produce elliptical galaxies. However, the importance and relative contributions of gaseous dissipation, isophotal shapes and kinematics is an area which has, and still continues, to generate some controversy. Gaseous dissipation has often been linked with mergers. For example, Mihos & Hernquist (1994); Springel (2000) included dissipation in their numerical simulations, which produced simulated merger remnants with "excess light" in their surface brightness profiles. This feature was later observed in one-third of the merger remnants in Rothberg & Joseph (2004), hereafter Paper I. Both numerical simulations (Barnes & Hernquist 1996; Barnes 2002) and observations (Wang, Schweizer, &

[1]Some of the data presented herein were obtained at the W.M. Keck Observatory, which is operated as a scientific partnership among the California Institute of Technology, the University of California and the National Aeronautics and Space Administration. The Observatory was made possible by the generous financial support of the W.M. Keck Foundation.

Scoville 1992; Whitmore et al. 1993) show that dissipation can lead to the formation of central gaseous disks which could later form stellar disks. The effects of gaseous dissipation were observationally inferred from the results in Rothberg & Joseph (2006), hereafter Paper II. The kinematic and photometric data showed that the central phase-space densities of the merger remnants were consistent with those of elliptical galaxies. One way to increase the phase-space density of spiral disks to match the levels in elliptical galaxies is a starburst induced by the dissipative collapse of gas (e.g. Negroponte & White (1983); Joseph & Wright (1985); Schweizer (1987); Barnes & Hernquist (1991); Kormendy & Sanders (1992); Mihos & Hernquist (1994, 1996)).

However, questions remain as to whether isophotal shapes are linked to specific formation scenarios. It has been argued that boxy ellipticals are also produced by mergers (Binney & Petrou 1985; Governato, Reduzzi, & Rampazzo 1993). Schweizer et al. (1990) even include boxiness in their definition of the fine structure index $\Sigma$, which they use to identify ellipticals with possible merger origins. Dissipationless (gas-free) merger models by Naab, Burkert, & Hernquist (1999) and Naab & Burkert (2003), hereafter NB03, show that equal-mass and some 2:1 mass ratio merger remnants can produce boxy shaped remnants which are anisotropically supported. A similar result was found for earlier numerical simulations by Heyl, Hernquist, & Spergel (1994). They concluded that the formation of elliptical galaxies via dissipationless merging does not lead preferentially to boxy or disky isophotes. All of these simulations found that viewing angle contributed significantly to whether a simulated merger remnant could be classified as boxy or disky. However, it is not clear what effect the presence of gas and star-formation may have on isophotal shapes or kinematics. There is some evidence that gas may suppress box orbits in mergers (Barnes & Hernquist 1996). New results from Naab et al. (2006) (hereafter N06), which include a non-star-forming gaseous component, indicate that 1:1 mass ratio merger remnants produce a wider range of kinematic properties, but seem more likely to have disky isophotal shapes.

The sample of advanced merger remnants presented in Papers I and II are ideal for testing the complicated and seemingly contradictory information offered by both numerical simulations and observations of elliptical galaxies. The *K*-band photometry from Paper I, in conjunction with the spectroscopic data (centered on the Ca triplet lines at $\lambda \sim 8500$ Å) from Paper II, will be used to measure the degree of rotational or anisotropic support in the merger remnants and compare that with their isophotal shapes and luminosity. The *K*-band is best suited for measuring the stellar component of mergers for two reasons. First, dust extinction is approximately one-tenth that at the *V*-band. Second, the blackbody emission of older, late-type stars, which trace the majority of the stellar mass in both elliptical and spiral galaxies, peaks in the near-infrared beyond 1 $\mu$m (Aaronson 1981). If mergers are undergoing star-formation, then the optical light is likely to be dominated by young stars and/or be heavily extincted. The Ca triplet lines were selected to measure stellar velocities

and dispersions because they are strong, well-separated, and narrow (Dressler 1984). Absorption lines at shorter wavelengths are more likely to be contaminated by strong nearby emission lines from galaxies undergoing star-formation or with young stellar populations, as well as more sensitive to template mismatch. Finally, the redward Ca triplet lines are somewhat less affected by extinction than absorption lines at shorter wavelengths.

The results will also be compared with real elliptical galaxies, primarily from BDM88 and B89, and numerical simulations of dissipationless merger remnants from NB03 along with simulated merger remnants with a gaseous component from N06. The goal is to test whether mergers are capable of forming boxy or disky (or both) elliptical galaxies. However, an important caveat to bear in mind is that the simulated merger remnants from NB03 are the result of purely stellar interactions and merging, while the results from Paper I and II indicate that the sample of observed merger remnants appear to be consistent with having undergone some form of gaseous dissipation and star-formation. Although N06 does include a gaseous component in the simulated merger remnants, the simulations do not include star-formation. The presence of star-formation could lead to differences between the observed and simulated merger remnants. All data and calculations presented in this paper assume a value of $H_\circ = 75$ km s$^{-1}$ Mpc$^{-1}$.

## 2. Samples

### 2.1. Merger Sample

The sample of merger remnants presented here is tailored to be reasonably large and to include only objects in the advanced stages of merging. The sample selection was based *solely* on optical morphology because, by definition, merger identification is a visual selection criterion. Selections based on other criteria, such as far-infrared luminosities, may introduce a bias into the sample towards objects undergoing star-formation. The 51 objects in the sample were chosen primarily from the Atlas of Peculiar Galaxies (Arp 1966), A Catalogue of Southern Peculiar Galaxies (Arp & Madore 1987), the Atlas and Catalog of Interacting Galaxies (Vorontsov-Velyaminov 1959), and the Uppsala General Catalogue (Nilson 1973). The full sample was selected based strictly on optical morphology and according to the following criteria:

1) Tidal tails, loops, and shells, which are induced by strong gravitational interaction.

2) A single nucleus, which, based on numerical studies, marks the completion of the merger. This criterion is important because it marks the point at which the merger should begin to exhibit properties in common with elliptical galaxies.

3) The absence of nearby companions which may induce the presence of tidal tails and

make the object appear to be in a more advanced stage of merging.

4) The merger remnants must be observable from Mauna Kea. This limited the survey to objects with declinations $\geq$ -50°.

Spectroscopic observations were made for a sub-sample of 38 objects. The sub-sample was not selected based on any particular criteria. Initially, spectroscopic observations were planned for all 51 objects in the sample, yet due to limitations of time, not all of the objects could be observed. While spectroscopic data were obtained for 38 objects, only 37 of these had sufficient signal-to-noise (S/N) to extract kinematic data spatially along the slit.

The merger remnants presented in this paper are listed in Table 1 which includes names, right ascension, declination and derived heliocentric recessional velocities. Since most of the objects have multiple designations, all subsequent references to sample galaxies within the paper, tables and figures will first use the NGC designation if available, followed by the Arp or Arp-Madore (AM), UGC, VV and lastly the IC designation if no other designation is available. Unless otherwise noted, the galaxies are listed in order of Right Ascension in tables and figures.

Within the merger sample there are three sub-samples, "shell ellipticals," Ultra-luminous and luminous infrared galaxies (ULIRG/LIRGs), and "normal merger remnants," which are defined simply as those galaxies which are neither ULIRG/LIRGs nor shell ellipticals. These distinctions are noted in Table 1. However, for the purposes of this paper, no distinction is made in the analysis among the sub-samples.

Table 1. Merger Kinematic Sub-Sample

| Merger Names | Other Names | R.A. (J2000) | Dec. (J2000) | $V_{\odot}$[a] (km s$^{-1}$) | notes |
|---|---|---|---|---|---|
| UGC 6 | VV 806 | $00^h\ 03^m\ 09^s$ | 21° 57′ 37″ | 6579 | LIRG |
| NGC 34 | VV 850 | $00^h\ 11^m\ 06^s$ | -12° 06′ 26″ | 5881 | LIRG |
| NGC 455 | Arp 164, UGC 815 | $01^h\ 15^m\ 57^s$ | 05° 10′ 43″ | 5827 | |
| NGC 1210 | AM 0304-255 | $03^h\ 06^m\ 45^s$ | -25° 42′ 59″ | 3878 | Shell |
| NGC 1614 | Arp 186 | $04^h\ 33^m\ 59^s$ | -08° 34′ 44″ | 4769 | LIRG |
| AM 0612-373 | ··· | $06^h\ 13^m\ 47^s$ | -37° 40′ 37″ | 9721 | |
| NGC 2418 | Arp 165, UGC 3931 | $07^h\ 36^m\ 37^s$ | 17° 53′ 02″ | 5037 | |
| NGC 2623 | Arp 243, UGC 4509, VV 79 | $08^h\ 38^m\ 24^s$ | 25° 45′ 17″ | 5549 | LIRG |
| UGC 4635 | ··· | $08^h\ 51^m\ 54^s$ | 40° 50′ 09″ | 8722 | |
| NGC 2655 | Arp 225, UGC 4637 | $08^h\ 55^m\ 37^s$ | 78° 13′ 23″ | 1400 | Shell |
| NGC 2782 | Arp 215, UGC 4862 | $09^h\ 14^m\ 05^s$ | 40° 06′ 49″ | 2543 | LIRG |
| NGC 2914 | Arp 137, UGC 5096 | $09^h\ 34^m\ 02^s$ | 10° 06′ 31″ | 3159 | |
| UGC 5101 | ··· | $09^h\ 35^m\ 51^s$ | 61° 21′ 11″ | 11802 | ULIRG |
| NGC 3256 | AM 1025-433, VV 65 | $10^h\ 27^m\ 51^s$ | -43° 54′ 14″ | 2795 | LIRG |
| Arp 156 | UGC 5814 | $10^h\ 42^m\ 38^s$ | 77° 29′ 41″ | 10738 | |
| NGC 3597 | AM 1112-232 | $11^h\ 14^m\ 41^s$ | -23° 43′ 39″ | 3500 | |
| NGC 3921 | Arp 224, UGC 6823, VV 31 | $11^h\ 51^m\ 06^s$ | 55° 04′ 43″ | 5896 | |
| NGC 4004 | UGC 6950, VV 230 | $11^h\ 58^m\ 05^s$ | 27° 52′ 44″ | 3368 | |
| NGC 4194 | Arp 160, UGC 7241, VV 261 | $12^h\ 14^m\ 09^s$ | 54° 31′ 36″ | 2501 | LIRG |
| NGC 4441 | UGC 7572 | $12^h\ 27^m\ 20^s$ | 64° 48′ 06″ | 2722 | |
| AM 1255-430 | ··· | $12^h\ 58^m\ 08^s$ | -43° 19′ 47″ | 8984 | |
| NGC 5018 | UGCA 335 | $13^h\ 13^m\ 00^s$ | -19° 31′ 05″ | 2816 | Shell |
| Arp 193 | UGC 8387, VV 821, IC 883 | $13^h\ 20^m\ 35^s$ | 34° 08′ 22″ | 6985 | LIRG |
| AM 1419-263 | ··· | $14^h\ 22^m\ 06^s$ | -26° 51′ 27″ | 6758 | |
| UGC 9829 | VV 847 | $15^h\ 23^m\ 01^s$ | -01° 20′ 50″ | 8465 | |
| NGC 6052 | Arp 209, UGC 10182, VV 86 | $16^h\ 05^m\ 12^s$ | 20° 32′ 32″ | 4739 | |
| UGC 10607 | VV 852, IC 4630 | $16^h\ 55^m\ 09^s$ | 26° 39′ 46″ | 10376 | |
| UGC 10675 | VV 805 | $17^h\ 03^m\ 15^s$ | 31° 27′ 29″ | 10179 | |
| AM 2038-382 | ··· | $20^h\ 41^m\ 13^s$ | -38° 11′ 36″ | 6092 | |
| AM 2055-425 | ··· | $20^h\ 58^m\ 26^s$ | -42° 39′ 00″ | 12890 | LIRG |

Table 1—Continued

| Merger Names | Other Names | R.A. (J2000) | Dec. (J2000) | $V_\odot$[a] (km s$^{-1}$) | notes |
|---|---|---|---|---|---|
| NGC 7135 | AM 2146-350, IC 5136 | $21^h\ 49^m\ 46^s$ | -34° 52′ 35″ | 2644 | |
| UGC 11905 | ··· | $22^h\ 05^m\ 54^s$ | 20° 38′ 22″ | 7456 | |
| NGC 7252 | Arp 226, AM 2217-245 | $22^h\ 20^m\ 44^s$ | -24° 40′ 41″ | 4792 | |
| AM 2246-490 | ··· | $22^h\ 49^m\ 39^s$ | -48° 50′ 58″ | 12901 | ULIRG |
| IC 5298 | ··· | $23^h\ 16^m\ 00^s$ | 25° 33′ 24″ | 8221 | LIRG |
| NGC 7585 | Arp 223 | $23^h\ 18^m\ 01^s$ | -04° 39′ 01″ | 3539 | Shell |
| NGC 7727 | Arp 222, VV 67 | $23^h\ 39^m\ 53^s$ | -12° 17′ 35″ | 1868 | |

Note. — (a) $\sigma_\circ$ (1.53 kpc aperture) measured from Ca triplet lines

### 2.2. Comparison Samples of Elliptical Galaxies and Simulated Merger Remnants

The same sets of kinematic and photometric properties presented in this paper for the observed merger remnants were extracted from a sample of 141 elliptical galaxies from Bender et al. (1988); Bender, Burstein, & Faber (1992); Bender, Saglia, & Gerhard (1994), and additional unpublished data from Bender. This is the same data set used by Naab et al. (1999), NB03 and N06 to compare with their numerical simulations. However, the data set did not include $K$-band photometry. Supplemental $K$-band data were obtained from the 2MASS archive, including the large galaxy atlas (Jarrett et al. 2003). A final sample of 84 elliptical galaxies, with measured values for all of the same parameters derived for the merger remnants, was compiled from the above data sets.

It is also important to briefly discuss the simulated merger remnants which are used as a comparison with the observed merger remnants presented in this paper. The photometric and kinematic parameters of the simulated remnants from NB03 were measured at a stage beyond which the bulge components of the progenitors have coalesced. Specifically, the simulated remnants merge at $t = 80$, where 1 time unit is $\sim 1.3{\times}10^7$ yrs. The simulations are allowed to evolve for 10 dynamical times ($\sim 10^8$ yrs or 70 time units). The evolution is then followed from $t =$ 150-200 to assure that no further evolution occurs. In the central regions, the dynamical times are shorter than $10^8$ years. The results of the simulations show little or no evolution after 150-200 time steps. The simulations are scale-free, therefore, if one assumes a smaller mass for the progenitors, the time units will scale appropriately.

The simulated merger remnants from N06 include a gas component. The remnants from NB03 were re-simulated with an additional gas component in the progenitor disk. Only 1:1 and 3:1 mass ratio simulations are presented here. 10% of the stellar disk in each progenitor was replaced by gas and the two progenitor disks were then merged in a fashion similar to NB03. The gas was represented by smooth particle hydrodynamics assuming an isothermal equation of state. This implies that additional heat created in shocks, adiabatic compression and feedback processes is radiated away immediately. No star-formation is included in the simulations. The merger remnants were allowed to settle into dynamical equilibrium for approximately 30 dynamical time-scales after the merger was complete, before their properties were measured.

The observed merger remnants have all been selected so that the sample only includes objects with a detectable single nucleus at $K$-band. Taking into account the effects of resolution and seeing, even the most distant merger remnant in the sample can be resolved down to a scale of $\sim$ 670 pc. Therefore, even if two nuclei are present but cannot be observationally separated, the *kinematic* properties should still be fairly close to their final values. Other numerical simulations have shown that kinematic properties (i.e. velocity dispersion)

settle to a constant value when the nuclei of the progenitors are at distances $< 1$ kpc (Mihos 1999). The observed merger remnants and the simulated merger remnants have ages which are consistent with each other. Regardless of how far along the merging process the observed remnants are, their kinematic properties are directly comparable to the simulated remnants because both samples have been "observed" after a stage in which these properties have been "frozen" into place. However, the photometric properties, such as ellipticity and isophotal shape may still be different. The results from Paper I indicate that while some of the remnants are devoid of central structure, not all appear to have fully phase mixed. Therefore, these properties may still be "in flux" as compared with the simulated remnants.

## 3. Observations

### 3.1. *K*-band imaging

Near-infrared images were obtained using the Quick Infrared Camera (QUIRC) 1024 × 1024 pixel HgCdTe infrared array (Hodapp et al. 1996) at the f/10 focus on the University of Hawaii 2.2 meter telescope. The field of view of the QUIRC array is 193″ x 193″ with a plate scale of 0.189″ pixel$^{-1}$. Details of how the observations were conducted can be found in Papers I and II.

The median seeing for the observations was 0″.8. The $K$ filter used in this survey for all but two objects conforms to the new Mauna Kea Infrared Filter Set (Tokunaga, Simons, & Vacca 2002). One object, UGC 6 was observed with the $K'$ filter (Wainscoat & Cowie 1992) and has been converted to $K$ using their conversion equation. Another object, IC 5298, was observed with an older $K$ filter with similar properties to the Mauna Kea $K$ filter. No conversion was made and it is assumed that $K_{old} \simeq K_{MaunaKea}$. Table 2 is the observation log for both the photometric and spectroscopic observations. Column (2) of Table 2 lists the total integration time for each object.

Table 2. Observation Log

| Merger Name | QUIRC Integration Time (sec) | ESI Integration Time (sec) | Slit P.A. (degrees) |
|---|---|---|---|
| UGC 6 | 3210 | 540 | 90.0 |
| NGC 34 | 3300 | 1200 | -41.0 |
| NGC 455 | 2250 | 1800 | -30.0 |
| NGC 1210 | 2820 | 300 | -41.0 |
| NGC 1614 | 2730 | 1800 | 32.9 |
| AM 0612-373 | 2160 | 1800 | 40.0 |
| NGC 2418 | 3600 | 1800 | 30.8 |
| NGC 2623 | 3390 | 1800 | 64.1 |
| UGC 4635 | 3480 | 1800 | 49.8 |
| NGC 2655 | 1800 | 1800 | 83.8 |
| NGC 2782 | 3000 | 1800 | 90.0 |
| NGC 2914 | 1800 | 1800 | 20.5 |
| UGC 5101 | 2700 | 1800 | 83.0 |
| NGC 3256 | 2925 | 629 | 0.0 |
| Arp 156 | 2400 | 3600 | -61.8 |
| NGC 3597 | 3300 | 1800 | 76.7 |
| NGC 3921 | 3645 | 1800 | 29.5 |
| NGC 4004 | 1560 | 1800 | -12.0 |
| NGC 4194 | 3600 | 1800 | -20.0 |
| NGC 4441 | 1440 | 1800 | 2.0 |
| AM 1255-430 | 3420 | 2700 | -77.2 |
| NGC 5018 | 2025 | 1140 | 90.0 |
| Arp 193 | 2625 | 3600 | -39.3 |
| AM 1419-263 | 3600 | 1800 | 69.0 |
| UGC 9829 | 3600 | 1800 | -15.0 |
| NGC 6052 | 3600 | 1800 | 71.5 |
| UGC 10607 | 3360 | 1800 | 0.0 |
| UGC 10675 | 3600 | 1800 | 90.0 |
| AM 2038-382 | 1920 | 1200 | -45.0 |
| AM 2055-425 | 2880 | 1200 | -35.0 |

Table 2—Continued

| Merger Name | QUIRC Integration Time (sec) | ESI Integration Time (sec) | Slit P.A. (degrees) |
|---|---|---|---|
| NGC 7135 | 2520 | 1800 | 0.0 |
| UGC 11905 | 3000 | 1200 | 49.5 |
| NGC 7252 | 3360 | 1800 | -60.0 |
| AM 2246-490 | 2520 | 1200 | -5.0 |
| IC 5298 | 3240 | 900 | 29.7 |
| NGC 7585 | 2040 | 900 | -70.0 |
| NGC 7727 | 3240 | 900 | 90.0 |

### 3.2. Optical Spectroscopy

The optical spectroscopic observations were obtained with the Echellette Spectrograph and Imager (Sheinis et al. 2002) at the W. M. Keck-II 10-meter telescope. The spectrograph covers the wavelength range from 3927-11068 Å. The observations were made in the echelle mode using the $0''.5 \times 20''$ slit, which corresponds to a resolution of $R \simeq 36.2$ km s$^{-1}$ or $R \simeq 8200$. The slit of the spectrograph was rotated to match the Position Angle (P.A.) of the major axis of each galaxy. The P.A. of the major axis for each galaxy was measured from the *K*-band photometric data. The total integration time and the P.A. of the major axis are listed in columns (3) and (4) of Table 2 respectively for each galaxy. In addition to spectrophotometric standards, giant stars covering the spectral range from G0III to M3III, and two super-giants of class M1Iab and M2Iab were observed with the same instrumental setup for use as template stars for the kinematic analysis. Paper II describes in more detail how the observations were conducted. The full list of template stars observed with ESI can be found in Table 3 of Paper II.

## 4. Data Reduction and Analysis

### 4.1. *K*-band imaging

The data set was reduced using IRAF. Structural photometric parameters were extracted from elliptical isophotes using the ELLIPSE task in the STSDAS package. The radius of each isophote was taken to be the measured seeing for that galaxy (i.e. the radius of the first isophote is the measured seeing). Paper I describes in detail the method used to extract the *K*-band photometric parameters. For the present paper only the ellipticity ($\epsilon$) and the $a_4/a$ parameter were used. The latter parameter is the amplitude of the cos $4\theta$ term, which measures the deviations of the isophote from a perfect ellipse. These two parameters were measured independent of any fits to the surface brightness profile of a galaxy. The ellipticity and $a_4/a$ parameters used in this paper were measured relative to the spatial scales of the kinematic observations. The values $\bar{\epsilon}$ and $\bar{a_4/a}$ were taken to be the average values *within the radius covered by the kinematic measurements*. These are the same definitions used in earlier kinematic studies of elliptical galaxies. Table 3 lists the measured *K*-band photometric parameters for each merger remnant along with derived spectroscopic parameters. The photometric parameters $\bar{\epsilon}$ and $\bar{a_4/a}$ are listed in columns (2) and (3) in Table 3 respectively.

The absolute magnitudes, $M_K$ were obtained by summing up the flux in circular apertures from the center to the edge of the array, after masking out foreground stars. This

method makes no assumptions about the profile shape of the galaxy. No corrections to the $K$-band data have been made for galactic extinction. Since the reddening at $K$ is very small, any such corrections, even for objects at low galactic latitude would be negligible. All distance dependent values listed in Table 3 assume a value of $H_\circ = 75$ km s$^{-1}$ Mpc$^{-1}$ and are derived using only the Heliocentric recessional velocities listed in Table 1. No additional corrections have been made. The values of $M_K$ are listed in column (4) of Table 3.

### 4.2. Optical Spectroscopy

Only the 7th order of the echellete spectra, containing the Ca triplet absorption line at $\lambda \simeq 8500$ Å, was analyzed for the data presented in this paper. The details of the data reduction are presented in Paper II. The only difference in the method of data reduction is that multiple one-dimensional spectra were extracted along the spatial axis. The aperture diameter of each extracted spectrum is equivalent to the measured seeing. The seeing was determined by taking the average FWHM of several stars in the acquisition camera. In cases where no acquisition camera images were saved, the FWHM along the spatial axis of the spectro-photometric standards or template stars closest in time to the galaxy observation were used.

The kinematic data were extracted from the spectra using the same method described in Paper II. A single stellar template was used in the fitting for each spectra extracted spatially along the slit. All of the stellar templates noted in Paper II were tested with each galaxy. The best fitting template for each galaxy was chosen based on the reduced chi-square and rms of the fit. The best-fit template star for each galaxy is listed in the last column of Table 3.

The errors shown in Table 3 are not absolute, and are provided more as reasonable estimates. The error analysis was conducted by testing various limits on the fitting process. First, Monte Carlo simulations were conducted to test the fitting program. The testing was based on 100 realizations of a template star convolved with a Gauss-Hermite polynomial of known properties with random noise added. This altered template star was used as a "test galaxy," to determine whether the fitting program could recover the input parameters. Next, a second template star of identical stellar type was used to recover the input parameters of the "test galaxy." The spread in errors from the Monte Carlo simulations were found to be nearly the same as the fitting errors determined by the program. Finally, template mis-match was tested by investigating the spread in the derived parameters from using different template stars. Only template stars which produced fits within $2\times{\chi_\nu}^2$ of the best-fitting template were used to test each galaxy. The largest errors in the fitting process were produced by template mismatch. The errors listed in Table 3 for the kinematic parameters

are the standard deviations of the derived parameters for the range of template stars used to test the mismatch.

The central velocity dispersions ($\sigma_\circ$) listed in column (5) of Table 3 were taken from Paper II. They were measured within an aperture diameter equivalent to 1.53 kpc (assuming $H_\circ = 75$ km s$^{-1}$ Mpc$^{-1}$ and using the heliocentric velocities measured in Table 1 for each object. This is equivalent to a $3\farcs4$ aperture at the distance of Coma. This aperture size was selected by Jorgensen, Franx, & Kjaergaard (1995); Smith et al. (1997) to bring spectroscopic measurements of $\sigma_\circ$ onto a common system.

The maximum observed rotation velocity ($V_m$) was measured for each galaxy. This parameter was measured by taking the average of the absolute values of the peak velocities of the left and right wings of the rotation curve. The values for each merger remnant are listed in column (6) of Table 3.

Table 3. Observed Kinematic and Structural Parameters

| Merger Name | $\bar{\epsilon}$ | $\bar{a_4}$ | $M_K$[a] | $\sigma_\circ$[b] (mag) | $V_m$ (km s $^{-1}$) | $V_m/\sigma_\circ$ (km s $^{-1}$) | $(V/\sigma)^*$ | Template Star[b] star/type |
|---|---|---|---|---|---|---|---|---|
| UGC 6 | 0.19 ± 0.01 | -0.00036 ± 0.01245 | -24.01 | 220 ± 10 | 60 ± 9 | 0.27 | 0.56 | HD 332389 G0III |
| NGC 34 | 0.11 ± 0.01 | 0.01361 ± 0.00882 | -24.61 | 201 ± 8 | 100 ± 4 | 0.49 | 1.41 | HD 332389 G0III |
| NGC 455 | 0.21 ± 0.01 | -0.00413 ± 0.00626 | -24.64 | 234 ± 7 | 132 ± 9 | 0.56 | 1.08 | HD 100059 K0III |
| NGC 1210 | 0.08 ± 0.01 | 0.00246 ± 0.00284 | -23.72 | 247 ± 6 | 34 ± 12 | 0.13 | 0.46 | HD 283778 M0III |
| NGC 1614 | 0.13 ± 0.02 | 0.00759 ± 0.01251 | -24.74 | 146 ± 12 | 108 ± 9 | 0.73 | 1.91 | HD 332389 G0III |
| AM 0612-373 | 0.11 ± 0.02 | -0.00643 ± 0.01605 | -25.65 | 303 ± 8 | 86 ± 8 | 0.28 | 0.80 | HD 99724 K3III |
| NGC 2418 | 0.16 ± 0.01 | -0.00249 ± 0.00403 | -25.31 | 288 ± 10 | 84 ± 7 | 0.29 | 0.66 | HD 100347 G8III |
| NGC 2623 | 0.24 ± 0.01 | 0.02390 ± 0.00956 | -24.22 | 191 ± 7 | 40 ± 4 | 0.20 | 0.37 | HD 100347 G8III |
| UGC 4635 | 0.34 ± 0.01 | 0.00757 ± 0.00403 | -24.71 | 251 ± 7 | 119 ± 10 | 0.47 | 0.65 | HD 100347 G8III |
| NGC 2655 | 0.19 ± 0.01 | 0.00047 ± 0.00598 | -23.70 | 169 ± 11 | 83 ± 6 | 0.49 | 1.00 | HD 100347 G8III |
| NGC 2782 | 0.26 ± 0.01 | 0.01028 ± 0.01193 | -23.83 | 196 ± 8 | 99 ± 7 | 0.50 | 0.85 | HD 100347 G8III |
| NGC 2914 | 0.35 ± 0.01 | 0.00684 ± 0.00431 | -23.51 | 186 ± 4 | 172 ± 2 | 0.92 | 1.26 | HD 100059 K0III |
| UGC 5101 | 0.18 ± 0.01 | 0.00622 ± 0.01132 | -25.50 | 287 ± 11 | 175 ± 6 | 0.60 | 1.29 | HD 100347 G8III |
| NGC 3256 | 0.19 ± 0.03 | 0.01348 ± 0.02181 | -24.72 | 241 ± 16 | 49 ± 7 | 0.20 | 0.41 | HD 100347 G8III |
| Arp 156 | 0.17 ± 0.01 | 0.01586 ± 0.01126 | -25.81 | 288 ± 8 | 157 ± 8 | 0.54 | 1.20 | HD 260158 K0III |
| NGC 3597 | 0.40 ± 0.01 | 0.01113 ± 0.01406 | -23.72 | 174 ± 9 | 140 ± 9 | 0.80 | 0.95 | HD 100347 G8III |
| NGC 3921 | 0.21 ± 0.01 | 0.00989 ± 0.00882 | -25.13 | 222 ± 5 | 117 ± 6 | 0.52 | 1.02 | HD 100347 G8III |
| NGC 4004 | 0.62 ± 0.01 | 0.02582 ± 0.02128 | -22.89 | 33 ± 2 | 20 ± 3 | 0.60 | 0.47 | HD 100347 G8III |
| NGC 4194 | 0.24 ± 0.02 | 0.00914 ± 0.01868 | -23.21 | 116 ± 7 | 81 ± 4 | 0.69 | 1.24 | HD 100347 G8III |
| NGC 4441 | 0.17 ± 0.01 | 0.00874 ± 0.00795 | -22.98 | 139 ± 6 | 60 ± 5 | 0.43 | 0.94 | HD 100347 G8III |
| AM 1255-430 | 0.28 ± 0.01 | -0.00645 ± 0.01063 | -24.93 | 243 ± 3 | 52 ± 8 | 0.21 | 0.33 | HD 99724 K3III |
| NGC 5018 | 0.25 ± 0.01 | 0.01175 ± 0.00324 | -25.15 | 222 ± 3 | 96 ± 6 | 0.43 | 0.74 | HD 100059 K0III |

Table 3—Continued

| Merger Name | $\bar{\epsilon}$ | $\bar{a_4}$ | $M_K$[a] | $\sigma_\circ$[b] (mag) | $V_m$ (km s $^{-1}$) | $V_m/\sigma_\circ$ (km s $^{-1}$) | $(V/\sigma)^*$ | Template Star[b] star/type |
|---|---|---|---|---|---|---|---|---|
| Arp 193 | 0.49 ± 0.01 | 0.00817 ± 0.01285 | -24.40 | 172 ± 8 | 111 ± 6 | 0.64 | 0.65 | HD 332389 G0III |
| AM 1419-263 | 0.27 ± 0.01 | 0.00375 ± 0.00581 | -24.94 | 260 ± 6 | 69 ± 10 | 0.26 | 0.43 | HD 100059 K0III |
| UGC 9829 | 0.41 ± 0.01 | 0.02622 ± 0.00965 | -24.96 | 134 ± 4 | 112 ± 6 | 0.83 | 1.00 | HD 100059 K0III |
| NGC 6052 | 0.44 ± 0.03 | 0.01377 ± 0.03115 | -23.55 | 80 ± 5 | 43 ± 4 | 0.53 | 0.60 | HD 100347 G8III |
| UGC 10607 | 0.24 ± 0.01 | 0.00256 ± 0.00590 | -25.20 | 211 ± 5 | 119 ± 4 | 0.56 | 0.99 | HD 100347 G8III |
| UGC 10675 | 0.18 ± 0.02 | 0.00724 ± 0.01413 | -24.80 | 177 ± 6 | 48 ± 7 | 0.27 | 0.57 | HD 100347 G8III |
| AM 2038-382 | 0.17 ± 0.01 | -0.00026 ± 0.00595 | -24.70 | 257 ± 8 | 142 ± 3 | 0.55 | 1.21 | HD 100347 G8III |
| AM 2055-425 | 0.05 ± 0.02 | 0.00751 ± 0.01598 | -25.08 | 185 ± 6 | 38 ± 7 | 0.20 | 0.88 | HD 332389 G0III |
| NGC 7135 | 0.18 ± 0.01 | 0.00393 ± 0.00474 | -23.95 | 277 ± 9 | 108 ± 3 | 0.38 | 0.82 | HD 100347 G8III |
| UGC 11905 | 0.24 ± 0.01 | -0.00762 ± 0.00626 | -24.51 | 222 ± 9 | 81 ± 6 | 0.36 | 0.64 | HD 100347 G8III |
| NGC 7252 | 0.07 ± 0.01 | 0.00236 ± 0.00820 | -24.84 | 166 ± 5 | 65 ± 4 | 0.39 | 1.42 | HD 100347 G8III |
| AM 2246-490 | 0.05 ± 0.02 | 0.00310 ± 0.01637 | -25.52 | 267 ± 7 | 34 ± 8 | 0.12 | 0.54 | HD 100347 G8III |
| IC 5298 | 0.08 ± 0.01 | 0.00807 ± 0.00722 | -24.92 | 193 ± 6 | 21 ± 5 | 0.10 | 0.36 | HD 100347 G8III |
| NGC 7585 | 0.29 ± 0.01 | 0.00328 ± 0.00499 | -24.98 | 211 ± 4 | 29 ± 7 | 0.13 | 0.21 | HD 100059 K0III |
| NGC 7727 | 0.24 ± 0.01 | -0.01634 ± 0.00936 | -24.23 | 231 ± 5 | 154 ± 5 | 0.66 | 1.18 | HD 99724 K3III |

Note. — All distance dependent values listed in Table 3 assume a value of $H_\circ = 75$ km s$^{-1}$ Mpc$^{-1}$ and are derived using only the Heliocentric recessional velocities listed in Table 1. No additional corrections have been made. (a) Data from Paper I. (b) Data from Paper II.

## 5. Results

In this section the photometric and spatially resolved kinematic properties of the observed merger remnants listed in Table 3 are compared with both simulated merger remnants (gas-free and with a gaseous non star-forming component) and a sample of 84 elliptical galaxies. In §5.1 the spatially resolved kinematics of the merger remnants are used to compare the rotational velocities with random motions to determine whether rotation or anisotropy is the dominant support mechanism. These results are then compared with both simulations and elliptical galaxies. Section 5.2 probes whether the merger remnants show the same correlations between kinematic and photometric properties, including shape and luminosity, as elliptical galaxies. These correlations are then tested against simulated merger remnants with and without a gaseous component. The simulations are also used to attempt to constrain the progenitor mass ratios of the merger remnants.

### 5.1. Are Merger Remnants Supported by Rotation or Anisotropy?

#### *5.1.1.* $V_m/\sigma_\circ$

One method of determining the amount of anisotropic or rotational support in an elliptical galaxy is the $V/\sigma$-$\epsilon$ plane. This measures the ratio of the maximum observed rotational velocity to the velocity dispersion compared with the ellipticity (Binney 1978). Figure 1 is a plot of $V_m/\sigma_\circ$ versus $\bar{\epsilon}$. This plot uses the central velocity dispersion $\sigma_\circ$ and mean ellipticity within the radius covered by the kinematic measurements. The choice in the particular ellipticity and velocity dispersion used is neccesitated by the need to compare the observed merger remnants with the same parameters used in the comparison sample of elliptical galaxies and numerical models. Furthermore, Binney (1981), suggests that the central velocity dispersion is the best measure of the velocity dispersion to compare with the rotational velocities. The superposed solid line is a model for an isotropically rotating oblate spheroid (Binney 1978). This line represents objects flattened by rotation as described by the tensor virial theorem. The equation of the line is:

$$(\frac{V}{\sigma})_{ISO} \simeq \sqrt{\frac{\epsilon}{(1-\epsilon)}} \tag{1}$$

from Kormendy (1982) and is a valid approximation for $0 < \epsilon < 0.95$. The dashed line is an approximation of the median value of an isotropic rotating *prolate* (tumbling end over end) spheroid (Binney 1978). If the sample objects were prolate, then half the points should lie above the line and half should lie below. Plotted in Figure 1 are the merger remnants (filled circles), the 84 galaxies from the comparison sample of ellipticals, and the probability con-

tours of the gas-free simulated merger remnants from NB03. The over-plotted ellipticals are divided by isophotal shape, open boxes are boxy ellipticals and open, flattened diamonds, are disky ellipticals. The probability contours of the simulated merger remnants are represented by three shades of gray, the lightest tone represents a 90% probability of finding a simulated merger remnant, the middle shade represent a 70% probability and the darkest shade a 50% probability. The figure is divided into four panels, each corresponding to the mass ratios of the simulated merger remnants from NB03. The mass ratios are noted in each panel.

The majority of merger remnants in Figure 1 appear to cluster close to the line of the isotropic rotating oblate spheroid. One-third of the merger remnants lie on or above the line. The distribution of merger remnants does not seem to be consistent with a prolate spheroid, as most of the points lie on or above the theoretical median line. Compared with the elliptical galaxies, the merger remnants show a similar range in ellipticities, but not in $V_m/\sigma_\circ$. There appears to be both an upper and lower limit. The merger remnants lie in a range of $0.10 \leq V_m/\sigma_\circ \leq 0.92$. This range is coincidental with only two-thirds of the ellipticals plotted in Figure 1. There are 19 ellipticals below the lower limit, all of which are boxy in shape and are the brightest ellipticals in the comparison sample. At the higher limit there are 10 ellipticals with $V_m/\sigma_\circ \geq 0.92$, all of which have disky isophotes.

In order to test whether a substantive difference in $V_m/\sigma_\circ$ values exists between the merger remnants and elliptical galaxies, a Kolmogorov-Smirnov (K-S) two-tailed test was employed. The K-S test probes the null hypothesis that the two distributions in question arise from the same parent population. It is a non-parametric test which makes no assumptions about the form of the parent distribution. The only assumption is that the two distributions are continuous. The results indicate that the null hypothesis can be rejected at better than the 0.02 significance level. However, while the K-S test is useful for detecting shifts in the probability distribution, it has difficulty detecting spreads in the distribution. Such spreads are most noticeable at the tails of the distribution (Press et al. 1992). A modified version of the K-S test developed by Kuiper is sensitive to changes at the tail ends of the distribution (Kuiper 1962; Stephens 1965). The Kuiper test indicates that the null hypothesis can be rejected at better than the 0.01 significance level. Thus, the the values of $V_m/\sigma_\circ$ for the merger remnants and elliptical galaxies do not arise from the same parent population. An additional item to keep in mind is the difference in sample sizes between the merger remnants and ellipticals (37 and 84 objects respectively). However, a comparison between the critical value, $D$, which is used for the both the K-S and Kuiper tests to determine at what significance level the null hypothesis can or cannot be rejected, produces only a very small difference between two equal samples of 84 objects and two samples, one of 37 objects and one of 84 objects.

This result seems to suggest that the difference in range of $V_m/\sigma_\circ$ values is real. It is possible that the lower limit of $V_m/\sigma_\circ$ may provide a means of discriminating between

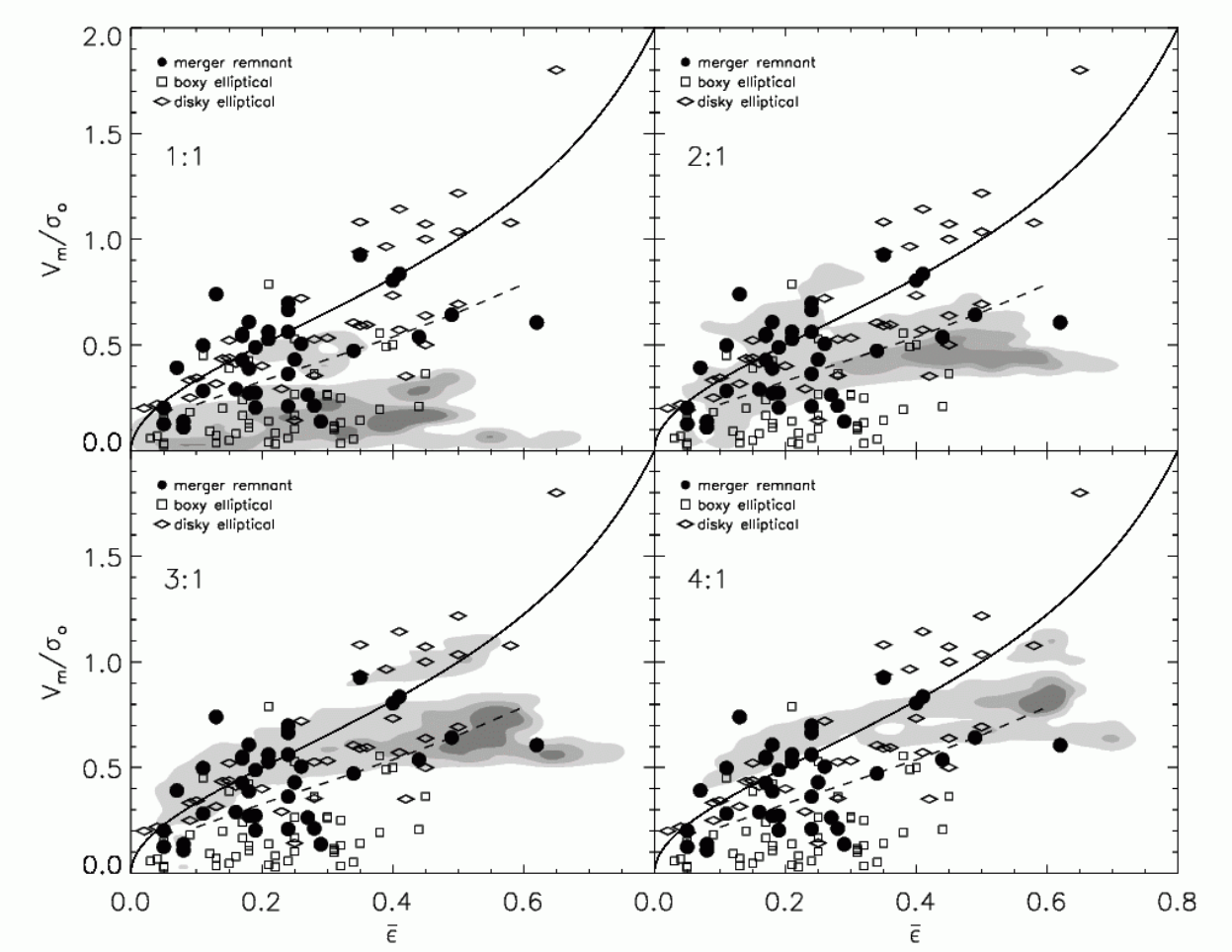



Fig. 1.— Diagram plotting the ratio of the maximum rotational velocity to the central velocity dispersion versus the mean ellipticity within the radius of the kinematic measurements. Plotted are the merger remnants (filled circles), the 84 galaxies from the comparison sample of ellipticals and the probability contours of the gas-free simulated merger remnants. The ellipticals are divided by isophotal shape, open boxes represent boxy ellipticals and open, flattened diamonds represent disky ellipticals. The probability contours of the simulated merger remnants are represented by three shades of gray, from light to dark representing a 90%, 70%, and 50% probability respectively of finding a simulated merger remnant. The solid line is a model of an isotropic rotating oblate spheroid and the dashed line is an approximation of the median value of an isotropic rotating prolate spheroid (Binney 1978). If the objects are prolate, then half should lie above the line and half should lie below. The figure is divided into four panels corresponding to 1:1, 2:1, 3:1 and 4:1 mass ratios of the progenitors of the simulated remnants.

bright ellipticals formed in a merger scenario and those possibly formed by slow buildup from accreting nearby galaxies or multiple mergers. The upper limit of $V_m/\sigma_\circ$ may also be a discriminant. All of these objects are disky ellipticals with lower luminosity. This is an interesting limitation in light of the results in which no *single-nuclei* merger remnants, either in this work, or the few previous observations (i.e. Lake & Dressler (1986) and Genzel et al. (2001)) have been observed to have a value of $V_m/\sigma_\circ > 0.92$.

The comparison between the simulated merger remnants and the observed merger remnants produces some surprising results. Only 20% of the observed merger remnants lie within the probability of the 1:1 mass-ratio simulated merger remnants. There is a far greater overlap between the 2:1 and 3:1 mass-ratio simulated merger remnants. This would *suggest* that the majority of the observed merger remnants stem from unequal mass mergers and are likely to be disky and rotationally supported. However, an important caveat to keep in mind is that while the simulated merger remnants are the result of dissipationless merging, the observed merger remnants show photometric and spectroscopic evidence of gaseous dissipation. As noted earlier, there is both numerical and observational evidence for the presence of gaseous disks in merger remnants. Springel (2000) noted a strong correlation between gaseous dissipation and disky isophotal shapes in his simulated merger remnants.

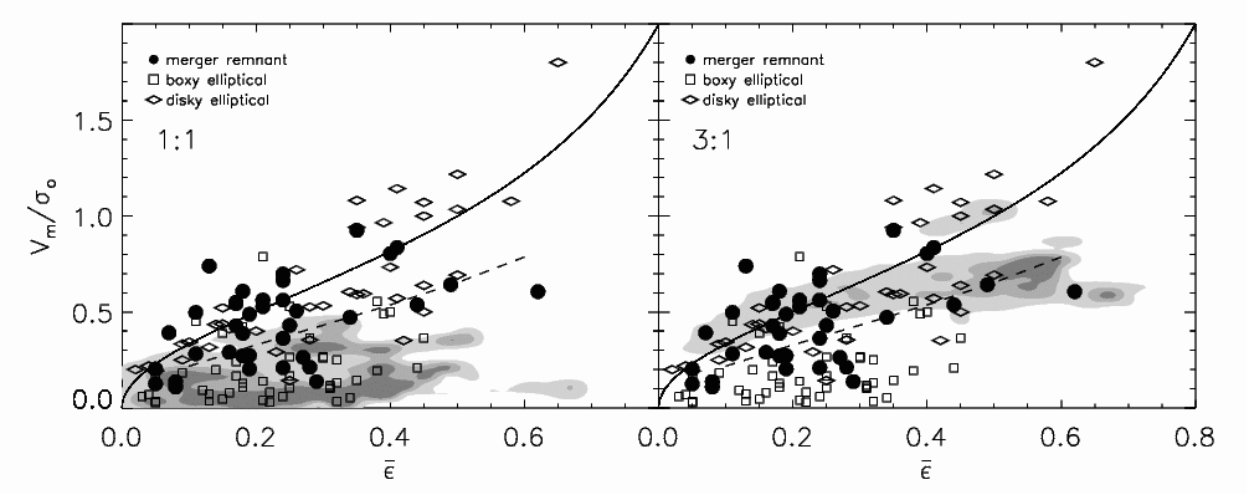



Fig. 2.— $V/\sigma$-$\epsilon$ plot comparing the merger remnants, elliptical galaxies and the simulated merger remnants with a gaseous component from N06. The symbols, overplotted lines and probability contours have the same meaning as in Figure 1.

Figure 2 shows a comparison between the simulated remnants from N06, which include a gas component, and the observed merger remnants. The symbols in Figure 2 have the same meaning as in Figure 1. Only 1:1 and 3:1 mass ratio simulated merger remnants are shown in Figure 2. The presence of a gaseous component in the simulated merger remnants does alter their observed parameters. Simulated merger remnants with 1:1 mass ratio progenitors now span a larger range of $V_m/\sigma_\circ$ values. The contours indicate that more of these simulated remnants can now be found closer to the line of an oblate isotropic rotator. The ellipticities lie within a smaller range (0-0.45) for values of $V_m/\sigma_\circ \leq 0.1$. As a result of these differences, more of the observed merger remnants now lie within the probability countours of the 1:1 mass ratio simulations and fewer lie within the probability contours of the 3:1 mass ratio simulations. This suggests that if the mergers contain a gaseous component, they are more in-line with equal mass ratio progenitors. These simulations do not account for the effects of star-formation, which may further alter the observed parameters. It is possible that once a star-formation component is taken into account, nearly all of the observed merger remnants could be consistent with equal mass ratio progenitors.

### *5.1.2. $(V/\sigma)^*$*

Another test of rotation versus anisotropy is to compare the measured $V_m/\sigma_\circ$ values with those from the isotropic rotating oblate models (the overplotted black line in Figure 1). This parameter is known as $(V/\sigma))^*$ and is defined by the following equation:

$$(\frac{V}{\sigma})^* = \frac{\frac{V_m}{\sigma_\circ}}{(\frac{V}{\sigma})_{ISO}} \tag{2}$$

where $(\frac{V}{\sigma})_{ISO}$ is the approximation noted above and defined by Kormendy (1982). A value of $(V/\sigma)^* = 1.0$ defines an object flattened by rotation, values of $(V/\sigma)^* \leq 0.7$ define anisotropically supported objects, and values between $0.7 < (V/\sigma)^* < 1.0$ define objects primarily supported by rotation (Bender 1988). $(V/\sigma)^*$ has been calculated for each merger and listed in column (9) of Table 3.

The results indicate that just over half of the merger remnants ($\sim 57\%$) appear to be supported primarily by rotation. When compared with the sample of ellipticals, the merger remnants show an apparent lower cutoff. No merger remnants in the sample have values of $(V/\sigma)^* < 0.21$. Unlike $V_m/\sigma_\circ$, there is no apparent cutoff for high values of $(V/\sigma)^*$.

Figure 3 shows a histogram distribution comparing the sample of 37 merger remnants with the 84 ellipticals galaxies in the comparison sample. The solid line is the distribution of ellipticals, the dashed line represents the merger remnants. The bin size is 0.1 and the histogram data are plotted to show the fraction of the total sample in each bin. The over-

plotted down arrows at the top of the histogram represent the peaks of the 1:1, 2:1, 3:1, and 4:1 mass ratio dissipationless simulations. The over-plotted up arrows at the bottom of the histogram represent the peaks of the 1:1 and 3:1 mass ratio simulations which contain a gaseous component. The ratios have been denoted with a $^\bullet$ to differentiate them from the gas-free simulations.

The distribution shapes do not appear to be similar. The elliptical galaxies peak at the smallest $(V/\sigma)^*$ values. The number of ellipticals as a fraction of the total sample decreases as the value of $(V/\sigma)^*$ increases. The merger remnants show a different distribution shape in $(V/\sigma)^*$. A K-S was used to test whether the merger remnants and ellipticals arise from the same parent population. The results indicate that at the 0.02 significance level the hypothesis can be rejected that the $(V/\sigma)^*$ distributions of the merger remnants and comparison sample of ellipticals arise from the same parent population. A Kuiper test was also employed for the reasons noted earler. The results are somewhat different. The hypothesis that the two populations arise from the same parent population can only be rejected at the 0.1 significance level.

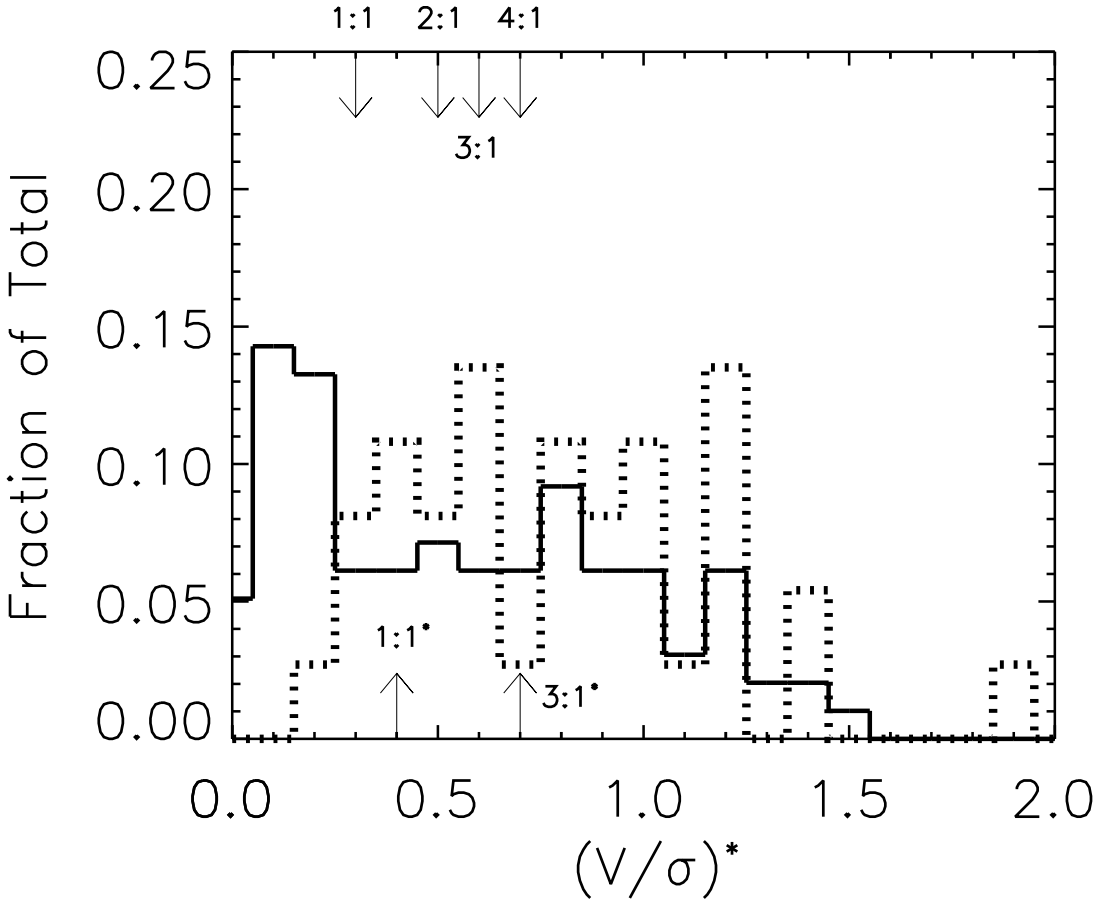



Fig. 3.— Histogram comparing the distributions of $(V/\sigma)^*$ between the sample of merger remnants (dashed line) and the comparison sample of elliptical galaxies (solid line). The bin size is 0.1 and the distributions are shown so that each bin is a fraction of the total. The over-plotted down arrows at the top of the histogram represent the peaks of the 1:1, 2:1, 3:1, and 4:1 mass ratio gas-free simulations. The over-plotted up arrows at the bottom of the histogram represent the peaks of the 1:1 and 3:1 mass ratio simulations which contain a gaseous component. The ratios have been denoted with a $^\bullet$ to differentiate them from the gas-free simulations.

The overall results of whether merger remnants are rotationally or anisotropically supported show that a majority of the sample appear to be flattened by rotation. A significant fraction of the sample do show evidence of anisotropic support. Furthermore, using both the $V_m/\sigma_\circ$-$\epsilon$ and $(V/\sigma)^*$ diagnostics, there appears to be a lower limit to the anisotropy present in merger remnants. No merger remnants lie below the values of $V_m/\sigma_\circ = 0.10$ and $(V/\sigma)^* = 0.21$. While it is possible that a much larger sample of merger remnants may include objects with these values, it is also possible that this represents a real physical limit. Thus, these parameters may be a viable method for distinguishing whether an elliptical galaxy was formed in a single merging event or a slow acrretion-driven buildup, possibly with multiple mergers, over a large period of time.

A comparison with the simulated dissipationless merger remnants from NB03 shows some differences as well. The 1:1 mass-ratio simulated merger remnants show a peak at $(V/\sigma)^* = 0.3$, with 80% having values $\leq 0.4$. The peak of the observed ellipticals lies is 0.1, while the merger remnants seem to have multiple peaks beyond 0.4. The 2:1, 3:1, and 4:1 mass ratio simulated remnants show peaks at $(V/\sigma)^* = 0.5$, 0.6, and 0.7 respectively. The simulated remnants with gas show a peak at 0.4 for 1:1 mass ratios and 0.7 for 3:1 mass ratios. As expected, these values are somewhat larger than the gas-free models. While the 1:1 mass-ratio simulations with gas are consistent with one of the peaks of the observed merger remnants, the remainder of the peaks do not overlap quite so well. The elliptical galaxies show a peak at a much smaller value of $(V/\sigma)^*$ than either the observed or simulated merger remnants. The gas-free simulations do not match well with the observed merger remnants.

## 5.2. Correlations Among Kinematics and *K*-Band Photometry

### *5.2.1. Rotation and Anisotropy vs. Shape*

It has been well established that elliptical galaxies show a strong correlation between $(V/\sigma)^*$ and $a_4/a$ (e.g. BDM88, B89, Kormendy & Bender (1996)). Anisotropically supported ellipticals have boxy isophotes, while rotationally supported ellipticals have disky isophotes. The correlation is not absolute, there are several examples of elliptical galaxies which run counter to this, however, over a large number of objects, it is considered to be a well defined trend. Figure 4 is a plot of the $(V/\sigma)^*$-$a_4/a$ plane for the merger sample, comparison sample of ellipticals and the dissipationless simulated merger remnants. The symbols are the same as in Figure 1. The vertical dashed line marks the separation between boxy (negative) and disky (positive) isophotal shapes. The horizontal dashed line marks the separation between anisotropically supported ($(V/\sigma)^* \leq 0.7$) and rotationally supported galaxies. The light, midtone, and dark gray contours represent the 90%, 70%, and 50% probability respectively

of finding a simulated merger remnant. The observed trend for ellipticals should place objects in either the bottom left quadrant or the top right quadrant.

More than half of the merger remnants follow the expected correlations; 4/37 are boxy and anisotropically supported and 17/37 are disky and rotationally supported. However, the merger remnants do show a somewhat wider dispersion in $a_4\bar{}/a$ compared with the ellitpical galaxies. In particular, 3 objects appear to be somewhat distant outliers as compared with both the elliptical galaxies and other merger remnants. The wider dispersion in $a_4\bar{}/a$ may be connected with the results of Paper I, specifically, that these objects have not fully phase mixed. A significant fraction of the sample do appear to have properties counter to the expected correlations, i.e. boxy and rotationally supported or disky and anisotropically supported. Yet, as can be seen from Figure 4, there are elliptical galaxies with similar properties. A comparison between these elliptical galaxies and merger remnants does show an interesting result. Twice as many merger remnants are disky and anisotropically supported as compared with elliptical galaxies. This is somewhat unusual, given that there are 2.2 times more elliptical galaxies than merger remnants.

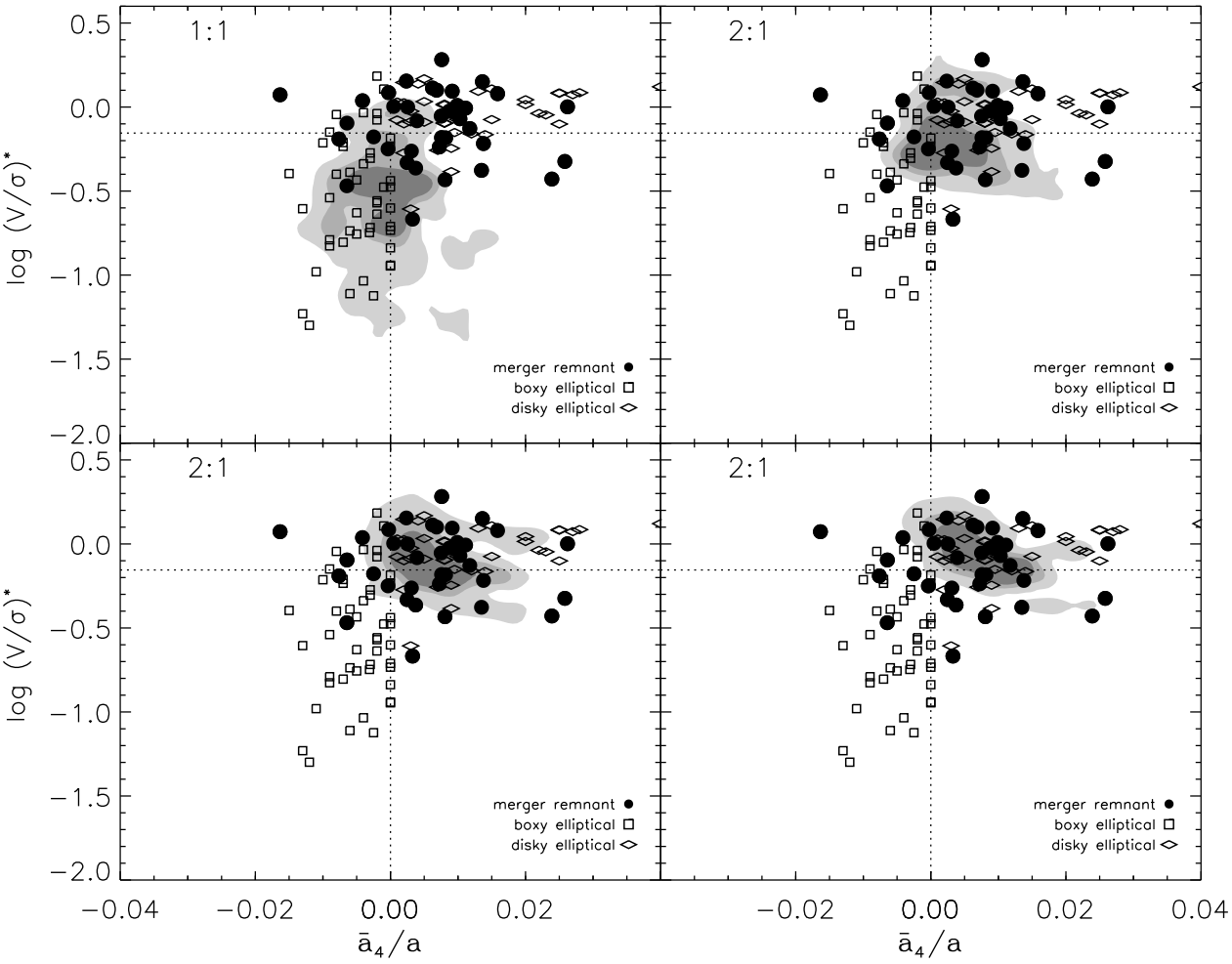



Fig. 4.— Plot showing the plane of isophotal shape versus versus the degree of rotational or anisotropical support ($(V/\sigma)^*$ versus $\bar{a_4}/a$). The symbols are the same as in Figure 1. The light, mid-tone and dark gray contours represent the 90%, 70%, and 50% probability respectively of finding a simulated dissipationless merger remnant from NB03.

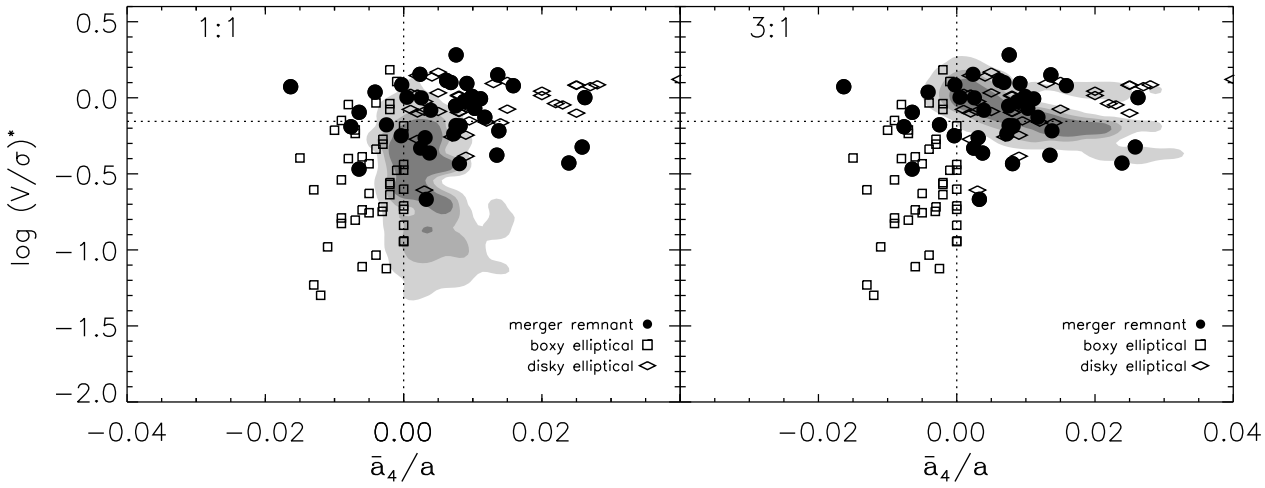



Fig. 5.— Similar plot to Figure 4, however, the contours represent the results from the N06 simulations which include a gaseous component.

When compared with the dissipationless simulated merger remnants, approximately one-third of the observed merger remnants overlap with the 1:1 mass-ratio simulated remnants. The 2:1 and 3:1 mass-ratio simulated remnants show a greater overlap with the observed merger remnants. This seems to suggest that the observed merger remnants are predominantly unequal mass in nature. However, NB03 do note an odd result in their models. They find that 28% of the 1:1 remnants appear to be disky, anisotropic system with the following properties: $a_4\bar{}/a > 0.003$ and $(V/\sigma)^* < 0.5$. Simulated merger remnants with these properties are defined as "forbidden" because they fail to resemble observed elliptical galaxies. Yet, 6/37 merger remnants have these observed properties.

While it is unlikely that the kinematics of the merger remnants will change once a single nucleus is formed (Barnes 1988, 1992; Mihos 1999), the results of Paper I indicate that phase mixing for the merger remnants is far from complete. This means that there is still some "memory" of the progenitor orbits remaining. In terms of the observed merger remnants, it is possible that these apparently contradictory properties are induced by gaseous dissipation which can modify isophotal shapes Barnes & Hernquist (1996). Once star-formation ceases and the merger becomes fully phase-mixed, the isophotal shapes may end up more in line with shapes expected from their kinematic properties.

Figure 5 is a similar plot to Figure 4, however, the simulated merger remnants shown are from N06. The symbols have the same meaning as in Figure 1 and only the 1:1 and 3:1 mass ratio simulated remnants are plotted. The most noticeable difference between the gas-free simulations and the ones with a gaseous component can be seen in the 1:1 mass ratio plot (Figure 5 *left*). The probability contours have shifted to the right. so that there is far less coverage where $a_4\bar{}/a \leq 0$ and more simulated remnants with values of $a_4\bar{}/a > 0$. The $(V/\sigma)^*$ values appear to be less affected by the gaseous component, although the contours now extend to slightly higher values. The inclusion of a gaseous component seems to produce remnants from equal mass mergers which, although containing signficant anisotropy, are quite disky in shape. This shift is better able to account for the observed merger remnants, especially those with so-called "forbidden" parameters (as noted above). The net result, however, is that far fewer of the 84 elliptical galaxies in the comparison sample now coincide with 1:1 mass ratio progenitors with gaseous components. The 3:1 mass ratio progenitors with a gaseous component now extend further into the disky $a_4\bar{}/a$ regime. However, the $(V/\sigma)^*$ values do appear to be affected. At smaller positive $a_4\bar{}/a$ values ($< 0.05$), the probability contours barely lie below $(V/\sigma)^* < 0.7$. The net result for the observed merger remnants, is that objects which had been consistent with dissipationless 3:1 mass ratio progenitors are now consistent with 1:1 mass ratio progenitors *with* a gaseous component. Moreover, between both the 1:1 and 3:1 mass ratio simulations with gas, practically all of the observed merger remnants with $a_4\bar{}/a > 0$ lie within one of the these probability contours. However, there are now several more mergers with $a_4\bar{}/a < 0$ which are not consistent with any of the simulations.

### *5.2.2. Rotation and Anisotropy vs. Luminosity*

Illingworth (1977) and Davies et al. (1983) found that a relationship exists between $M_B$ and both $V_m/\bar{\sigma}$ and $(V/\sigma)^*$. Faint ellipticals rotate more rapidly than bright ellipticals. However, Davies et al. (1983) noted that there was a larger scatter for bright ellipticals, possibly due to a combination of varying degrees of anisotropy and projection effects. Bender et al. (1989) noted a strong correlation between the $B$-Band luminosity and $\bar{a_4}/a$. Davies et al. (1983) predicted that if mergers form elliptical galaxies, then $V_m/\bar{\sigma}$ should decrease with increasing mass.

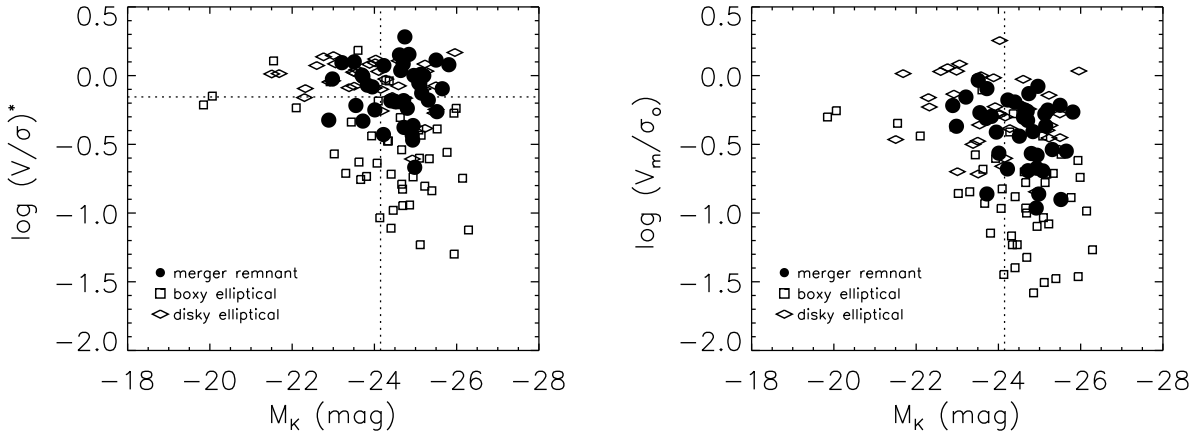



Fig. 6.— (a) *(left)* Plot of $K$-band absolute magnitude versus degree of anisotropy. Symbols are the same as in Figure 1. The $K$-band magnitudes for the ellipticals are taken from 2MASS. The horizontal dashed line at $(V/\sigma)^* = 0.7$ marks the transition between anisotropically and rotationally supported galaxies. The vertical dashed line at $M_K$ = -24.15 indicates the luminosity of a $1L^*$ elliptical galaxy (Kochanek et al. 2001). (b) *(right)* Plot of $K$-band absolute magnitude versus $V_m/\sigma_\circ$. Symbols are the same as in Figure 1. Again, the vertical dashed line at $M_K$ = -24.15 indicates the luminosity of a $1L^*$ elliptical galaxy.

Figures 6a and 6b show the $M_K$-log $(V/\sigma)^*$ and $M_K$-log $V_m/\sigma_\circ$ planes respectively for the merger sample and the 84 objects in the comparison sample of elliptical galaxies. The symbols are the same as in Figure 1. In Figure 6a, the horizontal dashed line at $(V/\sigma)^*$ = 0.7 marks the transition between anisotropically and rotationally supported galaxies. In both figures, The vertical dashed line at $M_K$ = -24.15 indicates the luminosity of a $1L^*$ elliptical galaxy (Kochanek et al. 2001), corrected to $H_\circ = 75$ km s$^{-1}$ Mpc$^{-1}$. A Spearman rank correlation test indicates that the elliptical galaxies show a strong anti-correlation (as luminosity increases both $V_m/\sigma_\circ$ and $(V/\sigma)^*$ decrease) at better than a 0.001 significance level for both $(V/\sigma)^*$ and $M_K$ and $V_m/\sigma_\circ$ and $M_K$. The merger remnants show no correlation (or anti-correlation) between $M_K$ and log $(V/\sigma)^*$ and a slight anti-correlation between $M_K$ and log $V_m/\sigma_\circ$ at the 0.1 significance level. This seems to weakly follow the prediction of Davies et al. (1983) that luminosity (and therefore mass) increases as objects become more anisotropic.

## 6. Summary and Discussion

The main results of this work are as follows:

1. More than half ($\sim$ 57 %) of the merger remnants exhibit properties consistent with the paradigm of boxy and anisotropic or disky and isotropic rotators: 4/37 are boxy and anisotropically supported; 17/37 are disky, and rotationally supported. However, the correlation with luminosity is less clear. Most (10/17) of the disky and rotationally supported merger remnants have luminosities $\geq 1L^*$. Yet, statistically, Figure 6b does indicate a weak anti-correlation between $K$-band luminosity and $V_m/\sigma_\circ$, suggesting that as mass increases the merger remnants are supported more by anisotropy. Figures 6a and 6b also show that compared with the elliptical galaxies, a higher fraction of the merger remnants have $K$-band luminosities $\geq 1L^*$.

2. Kinematically, the sample is split almost evenly between anisotropically supported (16/37) and rotationally supported (21/37) merger remnants. The discrepancy between the photometric and kinematic results may be due, in part, to the possibility that the isophotal shapes are still "in flux." This is consistent with the findings in Paper I, which showed that the most of the merger remnants in the sample have not fully phase-mixed. The kinematic properties may be close to, or at, their "final" values. This is supported by numerical simulations (Barnes 1988, 1992; Mihos 1999) which have shown that once a merger has coalesced to form a single nucleus, kinematic properties such as the velocity dispersion remain the same from that point onwards.

3. A significant fraction of the sample show trends counter to the expected correlation of boxy and anisotropic or disky and rotationally supported. The merger remnants show a

larger scatter in $\bar{a_4}/a$ compared with the elliptical galaxies. Three merger remnants appear to be outliers compared with the elliptical galaxy sample. An interesting result from the comparison with NB03, is that 1:1 mass ratio progenitors with so-called "forbidden" properties ($\bar{a_4}/a > 0.003$ and $(V/\sigma)^* < 0.5$) and which are not observed in elliptical galaxies, are found to exist in the observed merger remnant sample. 28% of the 1:1 mass ratio simulated merger remnants in NB03 lie in this "forbidden regime," as do 6/37 ($\sim 16\%$) observed merger remnants

4. The results suggest that the amount of anisotropy or pressure support in recent merger remnants is far less than in some old elliptical galaxies. There appears to be a clear line at $V_m/\sigma_\circ = 0.10$ and $(V/\sigma)^* = 0.21$ below which no merger remnants are found. This may be an observational tool which can be used to discern which ellipticals have been formed from disk-disk mergers.

5. When compared with *dissipationless* merger remnants, approximately one-third of the merger remnants are consistent with 1:1 mass progenitors, the rest are comparable, primarily, with 2:1 and 3:1 mass progenitors.

6. When the observed merger remnants are compared with the simulations that include a gaseous component, the fraction consistent with 1:1 mass ratio progenitors increases significantly. The simulations with a gaseous component appear consistent with remnants that have so-called "forbidden" parameters. The inclusion of a gaseous component appears to be more capable of accounting for observed merger remnants which are anisotropically supported, but have disky isophotal shapes. However, a consequence of this is that fewer boxy, anisotropically supported ellipticals are consistent with the newer simulations.

In the context of the Merger Hypothesis, a fundamental question to raise is: *How do merger remnants relate to the apparent dichotomy in elliptical galaxy types?* The photometry and kinematic results from Papers I and II support the idea that mergers are capable of forming elliptical galaxies. The data presented here appear to show that mergers can produce both rotationally and anisotropically supported systems. Papers I and II also suggest that most, if not all of the merger remnants have undergone some form of gaseous dissipation. Numerical simulations suggest that the effects of dissipation may contribute primarily to the formation of *disky* ellipticals (Barnes & Hernquist 1991, 1996; Springel 2000). In particular, the effects of dissipation can alter the stellar orbits, limiting or suppressing box orbits. This produces tube orbits which can lead to the formation of disky isophotal shapes. Springel (2000) modeled the effects of star-formation and feedback for use in hydrodynamical simulations of galaxy formation. The models cooled gas radiatively with a Schmidt-like star-formation rate and included the effects of feedback by supernovae. When applied to mergers of gaseous disk systems, the models produced a strong central starburst. The process of gaseous dissipation appeared to correlate with the presence of disky isophotes. Springel also included dissipationless disk-disk merger merger remnants as a comparison. Those produced

predominantly boxy isophotal shapes. However, like the results of NB03, viewing angle could make equal mass mergers appear either disky or boxy.

Moreover, Barnes (2002) found that dissipation builds rotating gaseous disks. Such gaseous disks have been confirmed observationally (e.g. Wang et al. (1992); Whitmore et al. (1993)) in some mergers. If these disks can form stars, it may explain both the disky isophotal shapes, as well as the apparent rotation observed in many of the merger remnants. These factors may contribute to the possible "lower-limit" in $(V/\sigma)^*$ observed in the merger remnants.

It has been previously suggested that mergers are incapable of forming giant elliptical galaxies (e.g. Shier & Fischer (1998); James et al. (1999); Colina et al. (2001); Genzel et al. (2001)). The photometry and kinematics presented in Papers I and II clearly challenge that assertion, as both the luminosity and kinematics of a significant number of the observed merger remnants are consistent with giant ellipticals. However, the largest measured $\sigma_\circ$ in the sample is 303 km s$^{-1}$, while observations of elliptical galaxies show objects with $\sigma_\circ >$ 350 km s$^{-1}$. These objects are almost exclusively bright and boxy in shape, with very small values of $(V/\sigma)^*$. Even the dissipationless 1:1 mass ratio simulations of NB03 do not appear to be consistent with the *most* massive giant ellipticals, and the N06 simulations with gas show even less overlap. All of these factors may point to some type of upper limit for the mass of an elliptical galaxy formed from disk-disk mergers. Other mechanisms, such as dissipationless mergers of bulge-dominated galaxies (Naab, Khochfar, & Burkert 2006) may be able to better reproduce the elliptical galaxies with the smallest $(V/\sigma)^*$ and most negative $\bar{a_4}/a$ parameters. However, this does raise a host of other problems, including reproducing the Fundamental Plane and $M_{BH}$-$\sigma_\circ$ relations (e.g. Nipoti, Londrillo, & Ciotti (2003); Kazantzidis et al. (2005)), as well as the presence of intermediate-age stellar populations and globular clusters in elliptical galaxies (e.g. Schweizer et al. (1990); Whitmore et al. (1997); Rejkuba et al. (2001); Whitmore et al. (2002); Thomas, Maraston, & Korn (2004); Goudfrooij et al. (2004); Trager et al. (2005)). Moreover, with recent deep surveys indicating the presence a red-sequence in color-magnitude diagrams of galaxies as far back as z $\sim$ 1 (Hogg et al. 2004; Bell et al. 2004; McIntosh et al. 2005), new questions have been raised concerning the limitations of disk-disk mergers versus other mechanisms, including dissipationless mergers between bulge-dominated galaxies. Future studies need to address the limitations of *both* merger scenarios to help constrain the importance and relative contribution of each to the formation of present day elliptical galaxies.

Another intriguing result, is that a significant fraction of the sample appear to show properties *contrary* to those expected of the boxy vs. disky elliptical paradigm. That is, a significant fraction show evidence of anisotropic kinematics, yet disky isophotal shapes, conversely, there are a few objects which show evidence of strong rotation, yet have boxy isophotes. The dissipationless merger models of NB03 also show similar results. They note

that 28% of the 1:1 remnants show unexpected properties, in particular, small $(V/\sigma)^*$ values with very disky isophotes. Further, they remark that the lack of *observed* merger remnants or elliptical galaxies with these properties may constitute a serious problem for the Merger Hypothesis. The results presented in this paper may indicate a reprieve for that possibility, as some real merger remnants clearly show these properties. Moreover, the newer simulations of N06, which include a gaseous component, appear to be more consistent with observed merger remnants which are disky and anisotropic. This raises several questions, such as why there are observed merger remnants as well as simulations with these properties, but relatively few or no elliptical galaxies. Are those types of elliptical galaxies still awaiting discovery? Or will the observed merger remnants evolve into elliptical galaxies with properties similar to those in present day ellipticals? How does the presence of star-formation and the evolution of the stellar populations fit into this situation? Perhaps future numerical simulations which can take into account both star-formation in the gaseous component and the evolution of the stellar populations can provide an answer.

Finally, a comparison between the simulated merger remnants from NB03 and N06 with the observed merger remnants presented here suggest that most of the sample are consistent either with dissipationless unequal mass mergers or equal mass mergers with a gasoues component. The latter is a more realistic result, given the supporting evidence from Papers I and II, and direct observations (e.g. Sanders et al. (1988); Dupraz et al. (1990); Wang, Scoville, & Sanders (1991); Casoli et al. (1991); Wang et al. (1992); Hibbard et al. (1994); Yun & Hibbard (2001); Wang et al. (2004)).

The results presented here would benefit from follow-up work. Most importantly, kinematic observations along the *minor* axis of the merger remnants would produce a stronger argument for or against rotational or anisotropic support. It would also help determine if any of the merger remnants are triaxial, which may explain some of the unexpected results. Additional kinematic observations out to larger radii along the major axis would help determine whether the observed $V_m/\sigma_\circ$ and $(V/\sigma)^*$ values are upper or lower limits. Finally, a more thorough analysis of both optical and infrared spectra can help confirm whether gaseous dissipation has occurred and the amount of star-formation present. These results can be used to constrain the evolution of the stellar populations in merger remnants, which, in conjunction with the kinematic results, can help address the question of whether these objects are capable of forming the most luminous and most massive elliptical galaxies.

We would like to thank Andreas Burkert and Thorsten Naab for providing data from their numerical models of dissipationless merger remnants as well as the data used to make comparisons with observed elliptical galaxies. A special thanks in particular is given to Thorsten Naab for sharing with us his latest unpublished results. These additional datasets

have helped to improve the quality of the work presented here. We would also like to thank Josh Barnes for informative discussions during the early stages of preparing this manuscript. A special thanks is given to Michael Cushing for his help and useful suggestions in developing the early versions of the IDL code used to derive the velocity dispersions from the extracted spectra. We thank Michael Connelley for taking $K$-band data of one of the mergers in the sample and Amy Apodaca for providing insight into some statistical issues, and finally, as always, a thanks to the back and forth nature provided by T. B. Wall. We would also like to thank the anonymous referee for comments and suggestions which have improved the manuscript. This research has made use of the NASA/IPAC Extragalactic Database (NED) which is operated by the Jet Propulsion Laboratory, California Institute of Technology, under contract with the National Aeronautics and Space Administration. This publication makes use of data products from the Two Micron All Sky Survey, which is a joint project of the University of Massachusetts and the Infrared Processing and Analysis Center, California Institute of Technology, funded by the National Aeronautics and Space Administration and the NSF. This research is supported in part, by a Fellowship from the NASA Graduate Student Researchers Program, Grant # NGT5-50396.

## REFERENCES

Aaronson, M. 1981, in IAU Symp. 96: Infrared Astronomy, 297–314

Arp, H. 1966, Atlas of Peculiar Galaxies (California Institute of Technology, Pasaadena, CA)

Arp, H. C. & Madore, B. F. 1987, A Catalog of Southern Peculiar Galaxies and Associations (Publisher: Cambridge University Press)

Barnes, J. E. 1988, ApJ, 331, 699

—. 1992, ApJ, 393, 484

—. 2002, MNRAS, 333, 481

Barnes, J. E. & Hernquist, L. 1996, ApJ, 471, 115

Barnes, J. E. & Hernquist, L. E. 1991, ApJ, 370, L65

Bell, E. F., Wolf, C., Meisenheimer, K., et al. 2004, ApJ, 608, 752

Bender, R. 1988, A&A, 193, L7

Bender, R., Burstein, D., & Faber, S. M. 1992, ApJ, 399, 462

Bender, R., Doebereiner, S., & Moellenhoff, C. 1988, A&AS, 74, 385, (BDM88)

Bender, R., Saglia, R. P., & Gerhard, O. E. 1994, MNRAS, 269, 785

Bender, R., Surma, P., Doebereiner, S., et al. 1989, A&A, 217, 35, (B89)

Binney, J. 1976, MNRAS, 177, 19

—. 1978, MNRAS, 183, 501

Binney, J. & Petrou, M. 1985, MNRAS, 214, 449

Binney, J. J. 1981, in Structure and Evolution of Normal Galaxies (Princeton University, New Observatory, Princeton NJ), 55–66

Carter, D. 1978, MNRAS, 182, 797

Casoli, F., Dupraz, C., Combes, F., et al. 1991, A&A, 251, 1

Colina, L., Borne, K., Bushouse, H., et al. 2001, ApJ, 563, 546

Davies, R. L., Efstathiou, G., Fall, S. M., et al. 1983, ApJ, 266, 41

Dressler, A. 1984, ApJ, 286, 97

Dupraz, C., Casoli, F., Combes, F., et al. 1990, A&A, 228, L5

Genzel, R., Tacconi, L. J., Rigopoulou, D., et al. 2001, ApJ, 563, 527

Goudfrooij, P., Gilmore, D., Whitmore, B. C., et al. 2004, ApJ, 613, L121

Governato, F., Reduzzi, L., & Rampazzo, R. 1993, MNRAS, 261, 379

Heyl, J. S., Hernquist, L., & Spergel, D. N. 1994, ApJ, 427, 165

Hibbard, J. E., Guhathakurta, P., van Gorkom, J. H., et al. 1994, AJ, 107, 67

Hodapp, K.-W., Hora, J. L., Hall, D. N. B., et al. 1996, New Astronomy, 1, 177

Hogg, D. W., Blanton, M. R., Brinchmann, J., et al. 2004, ApJ, 601, L29

Illingworth, G. 1977, ApJ, 218, L43

James, P., Bate, C., Wells, M., et al. 1999, MNRAS, 309, 585

Jarrett, T. H., Chester, T., Cutri, R., et al. 2003, AJ, 125, 525

Jorgensen, I., Franx, M., & Kjaergaard, P. 1995, MNRAS, 273, 1097

Joseph, R. D. & Wright, G. S. 1985, MNRAS, 214, 87

Kazantzidis, S., Mayer, L., Colpi, M., et al. 2005, ApJ, 623, L67

Kochanek, C. S., Pahre, M. A., Falco, E. E., et al. 2001, ApJ, 560, 566

Kormendy, J. 1982, in Saas-Fee Advanced Course 12: Morphology and Dynamics of Galaxies Saas-Fee Vol. 12: Morphology and Dynamics of Galaxies, p. 113

Kormendy, J. & Bender, R. 1996, ApJ, 464, L119+

Kormendy, J. & Djorgovski, S. 1989, ARA&A, 27, 235

Kormendy, J. & Sanders, D. B. 1992, ApJ, 390, L53

Kuiper, N. H. 1962, Proceedings of the Koninklijke Nederlandse Akademie van Wetenschappen series A, 63, 38

Lake, G. & Dressler, A. 1986, ApJ, 310, 605

Lauer, T. R. 1985, MNRAS, 216, 429

McIntosh, D. H., Bell, E. F., Rix, H.-W., et al. 2005, ApJ, 632, 191

Mihos, C. 1999, Ap&SS, 266, 195

Mihos, J. C. & Hernquist, L. 1994, ApJ, 437, L47

—. 1996, ApJ, 464, 641

Naab, T., et al. 2006, MNRAS, in preparation (N06)

Naab, T. & Burkert, A. 2003, ApJ, 597, 893, (NB03)

Naab, T., Burkert, A., & Hernquist, L. 1999, ApJ, 523, L133

Naab, T., Khochfar, S., & Burkert, A. 2006, ApJ, 636, L81

Negroponte, J. & White, S. D. M. 1983, MNRAS, 205, 1009

Nilson, P. 1973, Uppsala general catalogue of galaxies (Acta Universitatis Upsaliensis. Nova Acta Regiae Societatis Scientiarum Upsaliensis - Uppsala Astronomiska Observatoriums Annaler, Uppsala: Astronomiska Observatorium, 1973)

Nipoti, C., Londrillo, P., & Ciotti, L. 2003, MNRAS, 342, 501

Press, W. H., Teukolsky, S. A., Vetterling, W. T., et al. 1992, Numerical recipes in FORTRAN. The art of scientific computing (Cambridge: University Press, 2nd ed.)

Rejkuba, M., Minniti, D., Silva, D. R., et al. 2001, A&A, 379, 781

Rothberg, B. & Joseph, R. D. 2004, AJ, 128, 2098, (Paper I)

—. 2006, AJ, 131, 185, (Paper II)

Sanders, D. B., Soifer, B. T., Scoville, N. Z., et al. 1988, ApJ, 324, L55

Schweizer, F. 1987, in Nearly Normal Galaxies. From the Planck Time to the Present, p. 18

Schweizer, F., Seitzer, P., Faber, S. M., et al. 1990, ApJ, 364, L33

Sheinis, A. I., Bolte, M., Epps, H. W., et al. 2002, PASP, 114, 851

Shier, L. M. & Fischer, J. 1998, ApJ, 497, 163

Smith, R. J., Lucey, J. R., Steel, J., et al. 1997, MNRAS, 291, 461

Springel, V. 2000, MNRAS, 312, 859

Stephens, M. A. 1965, Biometricka, 52, 309

Thomas, D., Maraston, C., & Korn, A. 2004, MNRAS, 351, L19

Tokunaga, A. T., Simons, D. A., & Vacca, W. D. 2002, PASP, 114, 180

Toomre, A. 1977, in Evolution of Galaxies and Stellar Populations (New Haven: Yale Univ. Press), p. 401

Toomre, A. & Toomre, J. 1972, ApJ, 178, 623

Trager, S. C., Worthey, G., Faber, S. M., et al. 2005, MNRAS, 362, 2

Vorontsov-Velyaminov, B. 1959, Atlas and Catalog of interacting galaxies (Sternberg Institute, Moscow State University)

Wainscoat, R. J. & Cowie, L. L. 1992, AJ, 103, 332

Wang, J., Zhang, Q., Wang, Z., et al. 2004, ApJ, 616, L67

Wang, Z., Schweizer, F., & Scoville, N. Z. 1992, ApJ, 396, 510

Wang, Z., Scoville, N. Z., & Sanders, D. B. 1991, ApJ, 368, 112

Whitmore, B. C., Miller, B. W., Schweizer, F., et al. 1997, AJ, 114, 1797

Whitmore, B. C., Schweizer, F., Kundu, A., et al. 2002, AJ, 124, 147

Whitmore, B. C., Schweizer, F., Leitherer, C., et al. 1993, AJ, 106, 1354

Yun, M. S. & Hibbard, J. E. 2001, ApJ, 550, 104

This preprint was prepared with the AAS LaTeX macros v5.2.